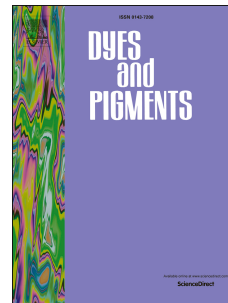


Accepted Manuscript

Synthesis and properties of bipolar derivatives of 1,3,5-triazine and carbazole

T. Matulaitis, N. Kostiv, J.V. Grazulevicius, L. Peciulyte, J. Simokaitiene, V. Jankauskas, B. Luszczynska, J. Ulanski



PII: S0143-7208(15)00428-3

DOI: [10.1016/j.dyepig.2015.11.001](https://doi.org/10.1016/j.dyepig.2015.11.001)

Reference: DYPI 4992

To appear in: *Dyes and Pigments*

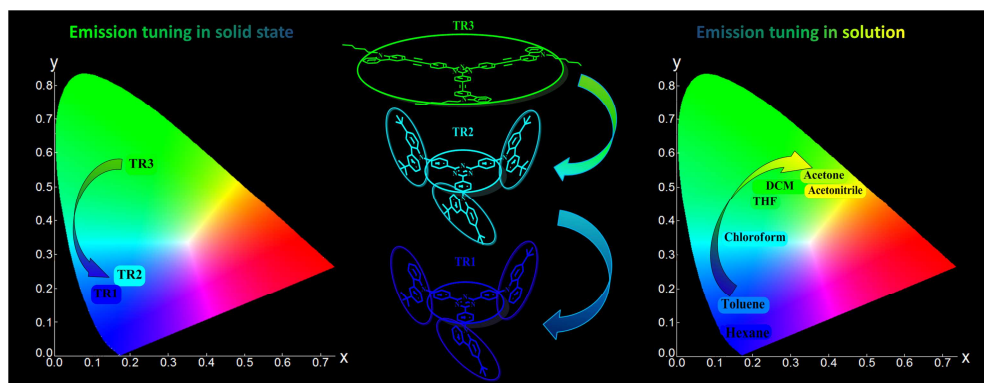
Received Date: 23 July 2015

Revised Date: 30 October 2015

Accepted Date: 2 November 2015

Please cite this article as: Matulaitis T, Kostiv N, Grazulevicius JV, Peciulyte L, Simokaitiene J, Jankauskas V, Luszczynska B, Ulanski J, Synthesis and properties of bipolar derivatives of 1,3,5-triazine and carbazole, *Dyes and Pigments* (2015), doi: 10.1016/j.dyepig.2015.11.001.

This is a PDF file of an unedited manuscript that has been accepted for publication. As a service to our customers we are providing this early version of the manuscript. The manuscript will undergo copyediting, typesetting, and review of the resulting proof before it is published in its final form. Please note that during the production process errors may be discovered which could affect the content, and all legal disclaimers that apply to the journal pertain.



Synthesis and properties of bipolar derivatives of 1,3,5-triazine and carbazole

T. Matulaitis^a, N. Kostiv^a, J. V. Grazulevicius^{a*}, L. Peciulyte^a, J. Simokaitiene^a, V. Jankauskas^b, B. Luszczynska^c, J. Ulanski^c

^aDepartment of Polymer Chemistry and Technology, Kaunas University of Technology, Radvilenu pl. 19, LT-50254, Kaunas, Lithuania, Fax: +37037 300152; Tel: +37037 300193

^bDepartment of Solid State Electronics, Vilnius University, Sauletekio al. 9, LT-10222, Vilnius, Lithuania

^c Department of Molecular Physics, Lodz University of Technology, Lodz, Poland

Abstract

Three new bipolar star-shaped derivatives of 2,4,6-triphenyl-1,3,5-triazine containing carbazolyl groups were designed, synthesized and characterized. All the materials possess high thermal stability and high glass transition temperatures ranging 97-226 °C. Photophysical study of the dilute solutions and neat films of the synthesized compounds was performed. Lippert-Mataga plots revealed linear dependence of Stokes shifts on the orientation polarizability for all the compounds. The dilute solutions of the triazine derivatives exhibited high photoluminescence quantum yields reaching 0.85, while for the neat films photoluminescence efficiency of 0.20-0.33 was observed. Ionization potentials of the solid layers of carbazole-triazine adducts estimated by photoelectron spectroscopy were found to be in the range of 5.49-5.97 eV. Hole drift mobility of the materials well exceeded the magnitude of $10^{-3} \text{ cm}^2 \text{ V}^{-1} \text{ s}^{-1}$ at an electric field of $6.4 \cdot 10^5 \text{ V/cm}$. The selected compounds were tested as light emitting materials in organic light emitting diodes based on host-guest systems.

Keywords

Triazine;

Carbazole;

* Corresponding author e-mail: juozas.grazulevicius@ktu.lt

Highlights

- Three carbazolyl containing 1,3,5-triazine derivatives were synthesized.
- The compounds exhibited superior thermal characteristics.
- The solvatochromic behavior was demonstrated.
- High photoluminescence quantum yields were observed for solutions and films.
- Blue and green OLEDs were fabricated.

1. Introduction

Organic conjugated materials have received great attention in recent decades in optoelectronic and electronic applications such as organic light-emitting diodes (OLEDs), organic solar cells, organic field effect transistors because of their potentially low cost and possibility of easy fabrication of the devices [1–4]. Recently, growing interest has been focused on the search of the materials with bipolar charge-transporting properties for the application in OLEDs [5,6]. Using bipolar materials for the preparation of emitting layers, enhanced performances and operational stability were demonstrated [7]. The utilization of bipolar materials also offers the possibility to achieve efficient and stable single-layer OLEDs, which are highly desirable because of simplification of the manufacturing process and reduction of the production costs [8].

The most widely adopted strategy to obtain bipolar materials is to incorporate D–A combinations into the same molecule, facilitating injection and transport of both holes and electrons [7,9,10]. Incorporation of electron-donating and electron-withdrawing moieties into a light-emitting material may promote the emission efficiency because of an extended π -conjugation. However, this might bring about a huge bathochromic effect. Therefore, one of the major challenges in developing bipolar blue emitters with D–A

structures is preventing the red-shift in the emission while maintaining or even increasing their photoluminescence quantum yield.

Compared to other donors, carbazole is useful in the generation of short-wavelength absorption and emission, as it is weaker π -donor than aromatic amines [11]. Bipolar hosts with carbazole as the donor moiety usually possess higher triplet energy than their counterparts with triphenylamino group. The triplet energy of carbazole ($T_1 = 3.19$ eV) is higher than that of triphenylamine ($T_1 = 3.04$ eV) [12]. Moreover, carbazole is a fully aromatic moiety providing high thermal, chemical and environmental stability [13]. It can be easily substituted with a wide variety of functional groups [14–16].

Triazine has an electron affinity larger than those of other typical electron-deficient heteroaromatic compounds (e.g., pyridine, pyrimidine) [17–19]. Due to this reason, triazine has been frequently incorporated into the backbone of conjugated compounds to improve their electron-injection and electron-transportation abilities [20–22]. In addition, derivatives of triazine exhibit good thermal stability [19]. Rigid skeleton of 2,4,6-triphenyl-1,3,5-triazine ensures high symmetry. Compounds containing triazine unit as electron-accepting center and carbazolyl or diphenylamino peripheral units linked through π -conjugated bridges showed aggregation induced emission and two-photon absorption properties [23].

In this paper we report on the synthesis of new star-shaped compounds containing both donor (carbazole) and acceptor (2,4,6-triphenyl-1,3,5-triazine) moieties linked through various linking bridges. We describe the results of optical, photophysical, electrochemical and computational studies which were carried out in order to study structure-properties relationship of these hybrid materials.

2. Experimental

2.1. Materials

Trifluoromethanesulphonic acid, copper iodide, *bis*-(triphenylphosphin)-palladium(II) dichloride ($\text{Pd}(\text{PPh}_3)_2\text{Cl}_2$), triphenylphosphine (PPh_3), trimethylsilylacetylene, triethylamine (Et_3N), tetrabutylammoniumhydrosulfate (TBAHS), 1-bromohexane, 1M tetrabutylammoniumfluoride (*n*- Bu_4NF) solution in THF, 4-iodobenzonitrile, aluminium trichloride (anhydrous), 18-crown-6, copper, sodium

ACCEPTED MANUSCRIPT
sulphate, 9H-carbazole, potassium iodide, potassium iodate, 2-chloro-2-methylpropane, acetic acid, sodium hydroxide, potassium carbonate were purchased from Sigma-Aldrich and used as received. Poly(N-vinyl carbazole) (PVK) and 2-(4-tert-butylphenyl)-5-(4-biphenyl)-1,3,4-oxadiazole (PBD) were also obtained from Aldrich. The solvents, i.e. toluene, chloroform, ethyl acetate, *n*-hexane, diethyl ether, methanol, acetone, acetonitrile, (Penta), dichloromethane (Poch), *o*-dichlorobenzene (Sigma–Aldrich) were dried and distilled according the conventional procedures [24].

2.2. Instrumentation

Nuclear magnetic resonance spectra of deuterated chloroform solutions of the synthesized compounds were recorded with a “Varian Gemini–2000” (300 MHz (¹H), 75.4 MHz (¹³C)) spectrometer. All the data are given as chemical shifts in δ (ppm), multiplicity, integration down field from (CH₃)₄Si as the internal standard. Mass spectra (MS) were obtained on “Waters ZQ 2000”. Elemental analysis data were obtained on a EuroEA Elemental Analyzer. Infrared (IR) spectra were recorded using “Perkin Elmer Spectrum GX II FT–IR System”. The spectra of the solid compounds were recorded in the form of KBr pellets.

UV–Vis spectra of 10⁻⁴ M solutions of the compounds were recorded in quartz cells using Perkin Elmer Lambda 35 spectrometer. Photoluminescence (PL) spectra of 10⁻⁵ M solutions of the compounds were recorded using Edinburgh Instruments’ FLS980 Fluorescence Spectrometer. Thin solid films for recording of UV–VIS and PL spectra were prepared by drop casting 2 mg/ml solutions of the compounds in toluene on the pre–cleaned quartz substrates. Fluorescence quantum yields (η) of the solutions and of the solid films were estimated using the integrated sphere method [25]. An integrating sphere (Edinburgh Instruments) coupled to the FLS980 spectrometer was calibrated with two standards: quinine sulfate in 0.1 M H₂SO₄ and rhodamine 6G in ethanol. Each quantum yield measurement was repeated 5 times and the error corridor was estimated. Fluorescence decay curves of the samples were recorded using a time–correlated single photon counting technique utilizing the nF920 Nanosecond Flashlamp as an excitation source. The phosphorescence spectra were recorded at 77 K for the solid solutions of the compounds (1 wt %) in Zeonex polymer matrix using nanosecond gated luminescence measurements (from 400 ps to 1 s) using a high energy pulsed Nd:YAG laser emitting at 355 nm (EKSPLA). A model liquid nitrogen cryostat (Janis Research) was used

for the experiment. The blue-edge highest energy peak in the phosphorescence spectrum was taken for the

ACCEPTED MANUSCRIPT

$T^1 \rightarrow S^0$ transition.

Differential scanning calorimetry (DSC) measurements were carried out with a TA Instruments “DSC Q100” calorimeter. The samples were heated at a scan rate of 10 °C/min under nitrogen atmosphere.

Thermogravimetric analysis (TGA) was performed on a “Mettler TGA/SDTA851e/LF/1100”. The samples were heated at a rate of 20 °C/min.

Ionization potentials (IP^{EP}) of the films of the synthesized compounds were measured by electron photoemission in air by the earlier reported procedure [26]. The materials were dissolved in chloroform and coated onto Al plates pre-coated with ~0.5 μm thick methylmethacrylate and methacrylic acid copolymer (MKM) adhesive layer. The function of MKM layer was not only to improve adhesion, but also to eliminate the electron photoemission from Al layer. In addition, this layer is conductive enough to avoid charge accumulation on it during the measurements. The measurement method was, in principle, similar to that described in literature [27]. The samples were illuminated with monochromatic light from the quartz monochromator. The negative voltage of -300 V was applied to the sample substrate. The counter-electrode with a slit for illumination was placed at ~5 mm distance from the sample surface. The counter-electrode was connected to the input of electrometer for the photocurrent measurement. The $I^{0.5} = f(h\nu)$ dependence was plotted. The linear part of this dependence was extrapolated to the $h\nu$ axis and the value was determined as the photon energy at the interception point. We evaluate the ionization potential measurement error as 0.03 eV.

Cyclic voltammetry (CV) measurements were carried out with a glassy carbon working electrode in a three-electrode cell using a μ-Autolab Type III (EcoChemie, Netherlands) potentiostat. Platinum wire and Ag/AgNO₃ (0.01 mol/l in acetonitrile) were used as counter and reference electrodes, respectively, and Bu₄NBF₆ in dichloromethane (0.1 M) was used as electrolyte. The data were collected using GPES (General Purpose Electrochemical System) software. Electrochemical measurements were conducted at room temperature at a potential rate of 100 mV/s. The reference electrode was calibrated versus ferrocene/ferrocenium redox couple. The solid state ionization potential energy (I_p^{CV}) was estimated from the onset oxidation potential by using the relationship $I_p^{CV} = 4.8 + E_{ox}$, where the potential is related to that

of ferrocenium/ferrocene. The electron affinity (EA^{SS}) values were obtained from the reduction potential using the approximation $EA^{CV} = 4.8 + E_{red}$.

Charge drift mobility measurements were performed by a xerographic time-of-flight (XTOF) method [28,29]. The samples for the charge mobility measurements were prepared as described earlier [30]. The samples for the measurements were prepared by drop-casting 10 mg/ml solutions of the compounds in $CHCl_3$ onto cleaned ITO coated glass substrate. After casting the cells were heated at 70 °C for 5 minutes. The charge carriers were generated at the layer surface by illumination with pulses of nitrogen laser (pulse duration was 1 ns, wavelength 337 nm). After photo excitation of the sample with a short light impulse, the rate of potential discharge in the XTOF measurements has a plateau region. The transit time was determined from the kink point in the transient photocurrent curves. The transit time t_{tr} with the surface potential (U_0) at the moment of illumination indicates the passage of holes through the entire thickness of the films (d) and enables determination of the hole mobility as $\mu = d^2/U_0 \cdot t_{tr}$. The experimental setup consists of a delay generator Stanford Research DG 535 and a digital storage oscilloscope Tektronix TDS754C.

The theoretical calculations were carried out using the Gaussian 09 quantum chemical package [31]. Full geometry optimizations of the compounds in their electronic ground state were performed with DFT using the B3LYP functional consisting of Becke's three parameter hybrid exchange functional combined with the Lee–Yang–Parr correlation functional with the 6-31G(d) basis set in vacuum. The energies of the highest occupied (HOMO) and the lowest unoccupied (LUMO) molecular orbitals were obtained from single point calculations in the framework of DFT B3LYP/6-311G(d,p) approach for the CH_2Cl_2 solution. Absorption spectra were simulated from the oscillator strengths of singlet transitions calculated by the TD-DFT B3LYP/6-31G(d) method in vacuum.

2.3. Synthesis

2,4,6-Tris(*p*-iodophenyl)-1,3,5-triazine (**1**) was prepared by the electrophilic cyclization reaction as described in the literature [32]. 3,6-Di-*tert*-butylcarbazole (**2**) and 3-*tert*-butylcarbazole (**3**) were obtained by the Friedel–Crafts alkylation according to the literature source [33]. The usage of iodination method of

Tucker yielded 3-iodocarbazole (**4**) [34]. 3-Iodo-9-hexylcarbazole (**5**), 3-(trimethylsilyl)ethynyl-9-hexylcarbazole (**6**) and 3-ethynyl-9-hexylcarbazole (**7**) were synthesized according the reported procedures [35].

2,4,6-Tris(4-(3-*tert*-butyl-carbazol-9-yl)phenyl)-1,3,5-triazine (TR1)

2,4,6-Tris(*p*-iodophenyl)1,3,5-triazine (**1**) (0.20 g, 0.29 mmol), 3-*tert*-butylcarbazole (**3**) (0.39 g, 1.75 mmol) and 18-crown-6 (0.02 g, 0.03 mmol) were dissolved in *o*-dichlorobenzene (10 mL) and the resulting solution was heated to reflux under nitrogen atmosphere. Then, K₂CO₃ (0.41 g, 0.99 mmol) and Cu (0.11 g, 0.58 mmol) were added. After being stirred for 24 h (TLC control), the reaction mixture was cooled down to the room temperature and filtered. The residue was carefully washed with chloroform and the solvent was evaporated under vacuum. The product was purified by silica gel column chromatography, using the mixture of hexane and dichloromethane in the volume ratio of 4:1 as an eluent, and recrystallized from the eluent mixture of solvents to afford the yellowish crystals (0.24 g, 43% yield). m.p. = 346–348 °C (DSC 344 °C). IR (KBr), ν/cm^{-1} : 3042, 2955, 2901, 2864, 1604, 1588, 1572, 1508, 1487, 1455, 1412, 1367, 1327, 1294, 1256, 1229, 1172, 1150, 1015, 813, 767, 744, 730, 636, 517. ¹H NMR (300 MHz, CDCl₃, δ ppm): 9.13 (d, 6H, J = 8.63 Hz, Ar); 8.25 (d, 3H, J = 4.17 Hz, Ar); 8.24 (d, 3H, J = 1.37 Hz, Ar); 7.92 (d, 6H, J = 8.64 Hz, Ar); 7.66 (d, 3H, J = 8.13 Hz, Ar); 7.60 (d, 6H, J = 1.04 Hz, Ar); 7.50 (td, 3H, J = 7.17 Hz, J = 1.17 Hz, Ar); 7.38 (td, 3H, J = 7.95 Hz, J = 0.86 Hz, Ar); 1.54 (s, 27H, CH₃-). ¹³C NMR (75.5 MHz, CDCl₃, δ ppm): 171.4, 143.9, 142.4, 140.8, 138.7, 134.6, 130.9, 126.7, 126.3, 124.4, 123.8, 120.6, 116.8, 110.2, 109.7, 35.1, 32.2. Elemental analysis found: C, 85.18; H, 6.20; N, 8.62%; molecular formula C₆₉H₆₀N₆ requires: C, 85.15; H, 6.21; N, 8.63%. MS (APCI⁺, 20 V), found: [M+H]⁺ m/z : 974; molecular formula C₆₉H₆₀N₆ requires: M = 973.29 g/mol.

2,4,6-Tris(4-(3,6-di-*tert*-butyl-carbazol-9-yl)phenyl)-1,3,5-triazine (TR2)

TR2 was prepared by the Ullmann coupling reaction from **1** (0.38 g, 0.55 mmol) and **2** (0.93 g, 3.32 mmol) using the same procedure as for the synthesis of **TR1**. The product was purified by silica gel column chromatography, using the mixture of hexane and dichloromethane in the volume ratio of 6:1 as an eluent, and recrystallized from the eluent mixture of solvents to afford the yellowish crystals (0.31 g, 49% yield). m.p. = 451–452 °C (DSC 448 °C). IR (KBr), ν/cm^{-1} : 3048, 2960, 2903, 2866, 1604, 1590, 1570, 1509, 1489, 1471, 1410, 1367, 1324, 1297, 1261, 1232, 1175, 1150, 1035, 1016, 878, 841, 810, 612. ^1H NMR (300 MHz, CDCl_3 , δ ppm): 9.11 (d, 6H, $J = 8.71$ Hz, Ar); 8.21 (dd, 6H, $J = 1.64$ Hz, $J = 0.85$ Hz, Ar); 7.89 (d, 6H, $J = 8.72$ Hz, Ar); 7.60 (d, 1H, $J = 0.74$ Hz, Ar); 7.57 (dd, 10H, $J = 1.86$ Hz, $J = 1.09$ Hz, Ar); 7.53 (d, 1H, $J = 1.75$ Hz, Ar); 1.52 (s, 54H, CH_3 -). ^{13}C NMR (75.5 MHz, CDCl_3 , δ ppm): 171.4, 143.7, 142.6, 140.7, 138.9, 134.38, 130.9, 126.5, 124.1, 124.0, 120.6, 116.6, 109.7, 35.1, 32.3. Elemental analysis found: C, 85.21; H, 7.44; N, 7.35%; molecular formula $\text{C}_{81}\text{H}_{84}\text{N}_6$ requires: C, 85.22; H, 7.42; N, 7.36%. MS (APCI⁺, 20 V), found: $[\text{M}+\text{H}]^+$ m/z : 1142; molecular formula $\text{C}_{81}\text{H}_{84}\text{N}_6$ requires: $M = 1141.61$ g/mol.

2,4,6-Tris(4-((9-hexyl-carbazol-3-yl)ethynyl)phenyl)-1,3,5-triazine (TR3)

Compound **1** (0.80 g, 1.16 mmol) was suspended in Et_3N (20 mL) in a dry 100 mL two-necked flask and the resulting mixture was heated to reflux under nitrogen atmosphere. Then, *bis*-(triphenylphosphin)-palladium (II) dichloride (0.05 g, 0.07 mmol), CuI (8.00 mg, 0.04 mmol) and 3-ethynyl-9-hexylcarbazole (**7**) (1.44 g, 5.24 mmol) were added. The reaction mixture was stirred for 24 hours at 90 °C. Then the solvent was evaporated under vacuum and the residue was extracted with chloroform. The organic phase was dried over anhydrous Na_2SO_4 . After evaporation of the solvents under reduced pressure the product was purified by silica gel column chromatography, using the mixture of hexane and chloroform in the volume ratio of 9:1 as an eluent, and precipitated into methanol to afford the yellowish solid (0.44 g, 34% yield). IR (KBr, cm^{-1}): $\nu = 3048, 2924, 2853, 2203, 1595, 1568, 1505, 1477, 1369, 1352, 1175, 1124, 813, 744, 726$. ^1H NMR (300 MHz, CDCl_3 , δ ppm): 8.77 (d, 6H, $J = 8.53$ Hz, Ar); 8.38 (d, 3H, $J = 1.35$ Hz, Ar); 8.14 (d, 3H, $J = 7.55$ Hz, Ar); 7.79 (d, 6H, $J = 8.55$ Hz, Ar); 7.73 (dd, 3H, $J = 8.48$ Hz, $J = 1.56$ Hz, Ar); 7.53 (t, 3H, $J = 7.04$ Hz, Ar); 7.44 (d, 3H, $J = 8.20$ Hz, Ar); 7.39 (d, 3H, $J = 8.62$ Hz, Ar) 7.30 (t, 3H, $J = 7.02$ Hz, Ar); 4.29

(t, 6H, $J = 7.08$ Hz, -N-CH₂-); 1.89 (quin, 6H, $J = 6.23$ Hz, -CH₂-); 1.29-1.45 (m, 18H, -CH₂-); 0.92 (t, 9H, $J = 6.86$ Hz, -CH₃). ¹³C NMR (75.5 MHz, CDCl₃, δ ppm): 171.2, 141.1, 140.5, 135.4, 131.8, 129.7, 129.1, 128.5, 126.4, 124.5, 123.1, 122.7, 120.8, 119.6, 113.1, 109.2, 109.0, 94.4 (-C \equiv C-), 88.1 (-C \equiv C-), 43.4 (-N-C-), 31.8, 29.2, 27.2, 22.8, 14.3. Elemental analysis found: C, 86.14; H, 6.41; N, 7.45%; molecular formula C₈₁H₇₂N₆ requires: C, 86.13; H, 6.43; N, 7.44%. MS (APCI⁺, 20 V), found: [M+H]⁺ m/z : 1130; molecular formula C₈₁H₇₂N₆ requires: M = 1129.52 g/mol.

2.4. Device fabrication

Electroluminescent devices were with the following configuration were fabricated: ITO/ poly 3,4-ethylenedioxythiophene:polystyrenesulfonate (PEDOT:PSS)/PVK:PBD (40 wt %): **TR2** (3 wt %)/LiF/Al (device I), ITO/PEDOT:PSS/PVK:PBD (40 wt %):**TR3**(3 wt %)/LiF/Al (device II). PEDOT:PSS was used for hole transport layer (HTL) (**Fig. S14**). The ITO-coated glass substrates were cleaned by ultrasonic treatment in the de-ionized water, acetone and isopropanol step by step during the 15 min for each solution. The layer of PEDOT:PSS was obtained on the glass substrate with ITO sublayer by spin coating of the 1:2 solution with methanol at the speed of substrate rotation of ca. 2000 rpm. The fabricated layer of PEDOT:PSS was dried at 200 °C for 10 min. The active light emitting layers PVK:PBD (60/40 wt %) doped by 3% of **TR2** or **TR3** with the thickness of 70 nm were spin coated from chlorobenzene solution on the top of PEDOT:PSS. The speed of substrate rotation was 2000 rpm and after 10 s was increased to 3000 for 10 s. After drying active the layers at 90°C for 30 min, the top electrode LiF/Al was deposited through the shadow mask by means of thermal vacuum evaporation at the pressure of ca. 10⁻⁵ Torr. The thicknesses of the layers were measured by profilometer (Dektak XT, Brucker).

The current density-voltage characteristics of the fabricated OLEDs were recorded by Keithley 2400 Source Meter. The luminance and color of the light emission of the fabricated devices were measured with the Minolta CS-200 camera. The electroluminescence spectra were recorded by MicroHR spectrometer and a CCD camera 3500 (Horriba Jobin Yvon). Photoluminescence spectra (PL) of the active layers containing **TR2** and **TR3** and without them were recovered by FLS980 fluorescence spectrometer with TMS300 monochromators and a red cooled detector (Hamamatsu R928P). The standard light source for measuring of

PL spectra was a 450 W xenon arc lamp. The absorption (UV) spectra of the films PVK:PBD,

ACCEPTED MANUSCRIPT

PVK:PBD:TR2, PVK:PBD:TR3 were recorded with the Cary 5000 UV–Vis–NIR spectrophotometer. All the measurements were carried out at the room temperature.

3. Results and discussion

3.1. Synthesis

Star-shaped derivatives of 2,4,6-triphenyl-1,3,5-triazine and carbazole were synthesized by the synthetic routes shown in **Scheme 1**. **TR1** and **TR2** were obtained by the three-step synthesis. At the first step, 4-iodobenzonitrile was subjected to cyclization with the help of trifluoromethanesulphonic acid to furnish 2,4,6-tris(*p*-iodophenyl)-1,3,5-triazine (**1**). At the second step alkylation of carbazole in the presence of 2-chloro-2-methylpropane and AlCl₃ was carried out. The alkylation products, 3,6-di-*tert*-butylcarbazole (**2**) and 3-*tert*-butylcarbazole (**3**), were isolated. At the final step, compound **1** and carbazole derivatives **2** and **3** were subjected to Ullmann coupling [36] to obtain the target compounds **TR1** and **TR2**. The synthetic route to compound **TR3** included five stages. Compound **7** was synthesized following the established routes and finally it was coupled with **1** by Hagihara–Sonogashira cross-coupling reaction [37] to afford the target product.

The chemical structures of the target compounds were identified by mass spectrometry, as well as IR and NMR spectroscopies and elemental analysis. The data were found to be in good agreement with the proposed structures. All the compounds exhibited characteristic signals at 171.2-171.4 ppm in ¹³C NMR spectra which can be attributed to the carbon atoms of the triazine heterocycle. For compounds **TR1** and **TR2** the characteristic singlet signal corresponding to the protons of methyl group of the *tert*-butyl moiety was found at 1.54-1.55 ppm in ¹H NMR spectra. Meanwhile, the carbon atoms of the ethynyl bridge linking the chromophores of **TR3** were characterized by the signals at 94.38 and 88.04 ppm in the ¹³C NMR spectrum and by absorption band at 2203 cm⁻¹ in the IR spectrum. Compounds **TR2** and **TR3** were found to be well soluble in common organic solvents, such as chloroform, THF, methylene chloride, while **TR1** was moderately soluble in the above mentioned solvents.

The temperature of the onset of thermal degradation and glass transition temperature (T_g) are important parameters of glass-forming organic semiconductors, since they provide information on the thermal and morphological stabilities of the active layers of the optoelectronic devices. The thermal properties of the synthesized star-shaped derivatives were investigated by the combination of DSC and TGA. All the target compounds exhibited very high thermal stability with the 5% weight loss temperatures exceeding 460 °C (see **Fig. S1**). Compounds **TR1** and **TR2** in which carbazole moiety contains branched *tert*-butyl groups exhibited superior thermal stability ($T_{d\text{TR1}} = 528$ °C and $T_{d\text{TR2}} = 514$ °C) with respect of compound **TR3** in which carbazole moiety contains long, linear hexyl group at N-9 position ($T_{d\text{TR3}} = 467$ °C). The values of the glass transition temperatures (T_g), melting temperatures (T_m), crystallization temperatures (T_{cr}) and the temperatures, at which initial loss of mass (5%) was observed (T_d) are summarized in **Table 1**.

DSC scans of **TR1-TR3** are presented in **Figs. S2-S4**. It was observed by DSC that both **TR1** and **TR2**, having one and two *tert*-butyl groups per carbazole moiety, respectively, can be transformed into the glassy state by cooling from the melt. They showed melting in the first heating scans but did not crystallize upon cooling. Compounds **TR1** and **TR2** exhibited glass transitions in the second DSC heating scans at 190 and 226 °C, respectively. Compound **TR3** was isolated after the synthesis as an amorphous substance. It did not show any melting or crystallization during the DSC experiment and exhibited only glass transition at 97 °C.

3.3. Optical and photophysical properties

UV-Vis absorption and fluorescence spectra of the dilute hexane solutions, as well as the spectra of the thin films of compounds **TR1-TR3** are presented in **Fig. 1**. The details of the optical and photophysical properties of the compounds are summarized in **Table 2**. The shape of absorption spectra of compounds **TR1** and **TR2** are similar, however the low-energy absorption maximum and the absorption edge of **TR2** exhibit small bathochromic shift with respect to those of **TR1**. This observation can apparently be explained by the larger amount of electron-donor *tert*-butyl groups in **TR2**. UV spectra of compounds **TR1** and **TR2** contain two well-expressed bands, while the spectra of compound **TR3** reflect three well-pronounced

transitions. A notable difference in the absorption spectra of **TR3** compared to those of **TR1** and **TR2** is that the oscillator strength of the low-energy absorption band of **TR3** is larger than those of **TR1** and **TR2** (see *chapter 3.6*). The larger oscillator strength suggests that there is a higher probability for the $S_0 \rightarrow {}^1CT$ transition in **TR3**. The highest-energy absorption bands of the studied derivatives can be associated with $\pi \rightarrow \pi^*$ transitions. For compounds **TR1** and **TR2** absorption shoulders located at 261 and 262 nm, respectively, correspond to the absorption of triphenyltriazine moiety [38]. For **TR3** this shoulder was observed only in the theoretical spectrum (**Fig. S18**). Absorption bands located in the range of 280–300 nm in the UV spectra of the investigated compounds can be attributed to a local excitation of the carbazole moiety [39]. The lowest-energy absorption bands located in the region of 340–430 nm can be assigned to the intramolecular charge transfer (ICT) complex transition $S_0 \rightarrow {}^1CT$. The similar tendencies were observed for the UV spectra of thin solid films. The shape of the absorption bands of the solid films of the derivatives was found to be similar to those of the solutions. However, the red shifts (up to 8 nm) and negligible broadening of the bands were observed indicating enhanced intermolecular interactions in the solid state.

UV and photoluminescence (PL) spectra of the dilute solutions of the studied compounds at room temperature revealed their solvent-dependant absorption and emission properties. In order to investigate solvatochromic effect UV and PL spectra of the dilute solutions of the compounds in the solvents of different polarity, i.e. hexane ($\epsilon = 1.88$), toluene ($\epsilon = 2.3$), chloroform ($\epsilon = 4.81$), tetrahydrofuran ($\epsilon = 7.6$), dichloromethane ($\epsilon = 8.93$), acetone ($\epsilon = 20.7$) and acetonitrile ($\epsilon = 37.5$), were recorded. The measurements performed for the solutions in the solvents of different polarity revealed small hypsochromic shifts of the lowest-energy absorption bands with the increase of solvent polarity for all the compounds investigated (see **Fig. S5**). We attribute these observations in the absorption spectra to the changes in the solvent refractive index n and the solute dipole moment [40].

Phosphorescence spectra of the solid solutions of compounds **TR1-TR3** in Zeonex polymer matrices were recorded at 77 K temperature (**Fig. 1**). All the phosphorescence spectra possess well-defined vibronic structures and are located in blue-green and green spectral regions. Since *tert*-butyl moiety is relatively weak donor, no significant differences between phosphorescence spectra of **TR1** and **TR2** were observed. The phosphorescence spectrum of **TR3** was found to be red-shifted, as compared to those of **TR1** and **TR2**. The

estimated values of triplet energy of **TR1-TR3** are presented in **Table 2**. They were found to be comparable for **TR1** and **TR2** (2.65-2.68 eV) and lower for **TR3** (2.38 eV).

Fig. 2 presents PL spectra of the solutions of **TR1** in various solvents (results for other compounds are given in **Fig. S6**). PL spectra of the solutions of all the compounds in hexane exhibited vibronic structures, consisting of two well-expressed maxima, which disappeared in the spectra of the solutions in more polar solvents. Disappearance of vibronic structure in polar solvents indicates that the photoexcited intramolecular charge transfer (ICT) from carbazolyl- to triazine moiety was enhanced when the polar solvents were used.

Solvatochromism is caused by the differential solvation of the ground state and the first excited state of the radiation-absorbing molecules [41]. With the increase of solvent polarity, the PL emission spectra of the studied compounds became broader and exhibited bathochromic shifts of 36-182 nm. This observation indicates that the dipole moments of all the compounds investigated are larger in the excited state than in the ground state (i.e. $\mu_e > \mu_g$). The differential solvation of the two states by solvents of varying polarity gives rise to an increase in the Stokes shift with increasing solvent polarity [42]. All the compounds exhibited positive solvatochromism. More precisely, the solvent relaxation process of the ICT fluorophore can be described by the Lippert–Mataga equation (1) [43,44]:

$$\Delta f = \frac{\epsilon-1}{2\cdot\epsilon+1} - \frac{n^2-1}{2\cdot n+1} \quad (1),$$

where Δf is defined as orientation polarizability, ϵ stands for a solvent dielectric constant, n corresponds to the refractive index of a solvent. The gap between the maximum of the first absorption band and the maximum of the corresponding fluorescence band is called the Stokes shift, and is usually expressed in wavenumbers as $\Delta\tilde{\nu} = \tilde{\nu}_a - \tilde{\nu}_f$. **Fig. 3b** shows linear relationship of Stokes shift of compound **TR1** on the orientation polarizability, Δf . This linearity indicates that the general solvent effects are dominant in the spectral shifts for all the compounds. All the studied compounds showed linear Stokes shift dependence on Δf , suggesting that they all are strong ICT fluorophores with highly localized excited state charge separation. In the case of **TR1** and **TR3**, the Stokes shift increased from 578 cm^{-1} and 377 cm^{-1} for the solutions in hexane to 8776 cm^{-1} and 8925 cm^{-1} for the solutions in acetonitrile, respectively. The largest Stokes shift was exhibited by **TR2**, varying from 616 cm^{-1} for the solution in hexane to 9843 cm^{-1} for the solution in

acetonitrile. This observation provides the further evidence of the larger excited-state dipole moment of **TR2** compared to those of **TR1** and **TR3**. These results are in agreement with those reported for the other bipolar triazine-based compounds [45–47].

Commission internationale de l'éclairage (CIE 1931) color coordinates (x, y) were calculated for the emission of the solutions and thin films of **TR1–TR3**. It was found that the solutions of all the studied compounds in non-polar hexane emit deep blue light (**Table 2, Figs. S9–S11**). With the increase of the polarity of solvents the emission of the solutions of the compounds shifts from deep blue through green up to yellow color. Estimation of chromaticity coordinates of the neat films of compounds **TR1–TR3** revealed that the emission of **TR1** and **TR2** remained blue, while the emission of **TR3** appeared in the green region. The different shift of the emission band of the film of **TR3**, as compared to those of **TR1** and **TR2**, can be explained by the different molecular packing in films. Compounds **TR1** and **TR2** contain bulky *tert*-butyl moieties, which provide high sterical hinderance, and thus more chaotic packing in the films. Meanwhile, all the aromatic part of **TR3** lies in one plane (see **Fig. S17**), which can result in more favourable molecular packing in the layer, leading to the stronger interaction (π - π stacking) between the molecules, which results in more pronounced bathochromic shift of the emission color.

PL quantum yield (η) gives the information on the efficiency of the emission process. It is defined as the ratio of the number of photons emitted to the number of photons absorbed [48]. PL quantum yields of the solutions of the investigated compounds in the solvents of the different polarity as well as of thin solid films were estimated using integrating sphere. **Fig. 3b** represents fluorescence quantum yield versus Δf plot for **TR1** (the plots for **TR2** and **TR3** are given in **Figs. S7b** and **S8b**). Generally, the η of the solutions of triazine derivatives **TR1–TR3** decreased with the increase of the solvent polarity. The PL quantum yields of **TR1** demonstrated linear dependance on orientation polarizability. PL quantum yield of 83% was observed for the solution in non-polar hexane, the lowest value of 23% was recorded for the solution in acetonitrile. Compounds **TR2** and **TR3** demonstrated the highest values of η of 80% and 85% in toluene solutions, while for the solutions in acetonitrile the values of η of 18% and 11% respectively were observed. With the increase of the solvent orientation polarizability (Δf), more time for a typical ICT fluorophore is required to reach its relaxed excited state, which enhances the non-radiative processes and leads to higher energy

losses. Therefore, the PL quantum yield is expected to decrease. PL efficiency of the solid films of **TR1** and **TR2** were found to be 33% and 29%, respectively, while that of the film of **TR3** was 20%. The details of the photophysical properties of the solutions of **TR1** in different solvents are summarized in **Table 3** (the data for the solutions of **TR2** and **TR3** are given in **Tables S1** and **S2**).

For more information on the dynamics of the $^1\text{CT}\rightarrow\text{S}_0$ emission, the PL decay curves of the dilute solutions of compounds **TR1–TR3** in the solvents of different polarity were recorded. The PL decays of the dilute solutions of all the compounds studied could be well described by single-exponential fits (except the solution of **TR3** in acetonitrile). The accuracy of the fits was characterized by χ^2 values of 1.00–1.08. With the increase of the solvent polarity from hexane to dichloromethane the solutions of all the compounds showed increasing values of fluorescence lifetime (τ), while τ of the solutions in acetone and acetonitrile were found to be 1–3 ns shorter, compared to those observed for the solutions in dichloromethane. τ of the solutions of **TR3** was found to be 2.7–3.5 times shorter than those of **TR1** and **TR2**. The shorter fluorescence lifetimes and higher PL quantum yields of the solutions of **TR3** as compared to those of the solutions of **TR1** and **TR2** shows that the $\text{S}_1\rightarrow\text{S}_0$ transition is dominant in **TR3**. This is in agreement with the significantly higher (by 2.7–3.0 times) oscillator strength of the transition $\text{S}_0\rightarrow\text{S}_1$ observed in the UV spectrum of the solution of **TR3** as compared with those of the solutions of **TR1** and **TR2**.

To evaluate the contributions of radiative and nonradiative decay processes in the solutions of the studied compounds, radiative and nonradiative decay rates, Γ and k_{NR} , respectively, were estimated [49]. Γ decreased exponentially with the increase of solvent polarity for the solutions of all the compounds (for **TR1** see **Fig. 3a**, for **TR2** and **TR3** see **Figs. S7a** and **S8a**). For the solutions of **TR3** the values of Γ were found to be by ca. 3 times higher than those of the solutions **TR1** and **TR2**. This observation is consistent with larger oscillator strength of the $\text{S}_0\rightarrow\text{S}_1$ transition in the UV spectrum of **TR3**. The rate of k_{NR} increased with the increase of the solvent polarity, indicating the enhancement of the non-radiative processes. This observation is consistent with the decrease of PL quantum yields with the increase of the solvent polarity.

Fluorescence decays of the neat films exhibited nonexponential behavior, pointing out several different origins of the radiative transitions (**Fig. 4**). PL decays of the compounds investigated in the solid state were best described by biexponential fits (see **Table 2**). The emission of the film of **TR1** had dominant τ of 1.05

ns (67%) and also exhibited fluorescence of long-lived excited state species with a τ of 4.70 ns. The neat films of **TR2** and **TR3** demonstrated almost equal contribution of short-lived 1.29 ns and 1.38 ns for **TR2** and **TR3**, respectively, and of long-lived excited state species with τ of 5.27 ns and 4.56 ns, respectively. To our mind, the large difference between the dominant PL lifetimes of the all the compounds in solution and solid state suggests complications due to intermolecular interactions or morphology, or can be a consequence of different CT species in different solid-state conformations.

3.4. Electrochemical properties

Electrochemical properties of **TR1–TR3** were studied by CV in order to elucidate the electronic energy levels which determine the energy and electron transfer processes and reversibility of redox processes. **Figure 5** illustrates the CV graphs of compounds **TR1–TR3**. Only **TR2** showed reversible oxidation at 1.10 V during CV experiment. Since compounds **TR1** and **TR3** contain unsubstituted active C-6 positions of carbazole moieties, they showed irreversible oxidation processes at 0.89 V for **TR1** and at 0.77 V for **TR3**. The similar observations were reported earlier [50,51]. For such compounds growing peak of current during the CV experiment and the resulting formation and growth of thin films on the working electrode demonstrate the occurrence of oxidation induced electropolymerization [52,53]. Compounds **TR1** and **TR2**, in which the carbazole moiety is linked to triazine core through N-9 position of carbazole moiety, demonstrated reversible reduction at -1.74 V and -1.77 V respectively. This observation shows that in these conditions a stable radical anion is formed on the triphenyltriazine moiety [54]. **TR3** did not exhibit any notable reduction peak during the CV experiments.

Solid-state ionization potential is a useful parameter for organic semiconducting materials for the use in optoelectronic applications. Solid state ionization potential (IP^{CV}) and electron affinity (EA^{CV}) values of the synthesized compounds were estimated using ferrocene/ferrocenium as the standard redox system. The half wave potentials and IP^{CV} and EA^{CV} values are summarized in **Table 4**. Compound **TR2** was found to possess the highest IP^{CV} value of 5.70 eV, while compound **TR3** demonstrated the highest electron donating ability showing the value of IP^{CV} of 5.37 eV.

The ionization potentials (IP^{EP}) of the solid samples of **TR1–TR3** were also measured by the electron photoemission in air method. The electron photoemission spectra of the layers of **TR1–TR3** are shown in **Fig. S12**. The values of IP^{EP} are presented in **Table 4**. The IP^{EP} values were found to be by 0.12 – 0.46 eV higher than the IP^{CV} values of the corresponding compounds. However both the methods revealed the same trend. The lowest IP values were recorded for **TR3** while the highest values were observed for **TR2**. The small differences between the values of IP obtained by electron photoemission spectrometry and by electrochemical studies are apparently due to the difference in molecular interactions and molecular arrangements in the solid layers and in dilute solutions of the derivatives.

3.6. Theoretical calculations

The DFT approach [55] was applied for the interpretation of the structure–property relationship of **TR1–TR3**. DFT calculations were performed using the Gaussian suite of programs (Gaussian 09W) [31]. The geometries were optimized in the ground state using basic restricted DFT B3LYP 6-31G(d) basis set in vacuum. Our calculations show that the optimal neutral electronic ground state geometries are not planar for the molecules of **TR1** and **TR2**. The B3LYP ground state geometry shows a torsional angle of ca. 48° between carbazole and phenylene fragments. The presence of ethynyl linker in the molecule of **TR3** forbids rotations around it. Therefore mutual orientation of lateral fragments with respect to the ethynyl linker is of ca. 0.23°. The analysis of the optimized bond lengths in the electronic ground state obtained at the B3LYP theoretical level for all three molecules revealed the similar bond lengths, with the smallest values observed for **TR3**. The geometry optimizations for the molecules of **TR1–TR3** can be found in **Figure S17**.

In order to estimate the role of 1,3,5-triazine–based star–shaped structure on the optical transitions, the occupied and the unoccupied molecular orbitals contributing to the lowest energy electronic transitions were studied using time–dependent version of DFT method (TD–DFT) [56]. Absorption spectra were simulated from the oscillator strengths of singlet transitions calculated by the TD–DFT B3LYP/6-31G(d) method in vacuum. Two dominant transitions are observed in the absorption spectra of compounds **TR1** and **TR2** (**Fig. S17**), which can be attributed to the transition $S_0 \rightarrow S_1$, with the oscillator strengths of 0.55 for **TR1** and of

0.60 for **TR2**, and $\pi \rightarrow \pi^*$ transitions with the oscillator strengths of 0.43 for **TR1** and of 0.48 for **TR2**. The theoretical simulation of the vertical transitions of **TR3** revealed that there is larger contribution of $\pi \rightarrow \pi^*$ transitions during the excitation of this compound, as compared to the other two compounds. The highest intensity absorption band appears from the $S_0 \rightarrow S_1$ transition with the oscillator strength of 1.65.

Figure 6 shows the frontier orbitals of the investigated molecules. In the case of **TR1** and **TR2**, the HOMO orbitals are delocalized over all three phenylene–carbazole fragments and the lobes are perpendicularly oriented to C-N bonds linked to these chromophores. The similar tendencies were observed for **TR3**. The HOMO orbitals of **TR3** are also delocalized over all three carbazole–acetylene–phenylene fragments. In all three molecules the LUMO orbitals are localized mostly over the central triphenyltriazine part. The lobes of these orbitals show the inter–ring bonding character. The HOMO orbitals also indicate that the electron distraction from the molecule will be connected with the electronic structure changes on the terminal carbazole fragments. On the other hand, the electron reduction, affects mostly the 2,4,6-triphenyl-1,3,5-triazine moiety.

3.7. Charge–transporting properties

Xerographic time–of–flight measurements were used to characterize the charge–transporting properties of the synthesized compounds. Investigations were carried out for the layers of **TR1–TR3** coated on aluminum plated glasses by solution processing technique. The photogeneration quantum efficiency of holes was estimated from the magnitude of extracted charge in XTOF experiment after excitation of samples with short nitrogen laser light pulse ($\lambda = 337$ nm, duration – 1 ns). **Figure 7** shows the electric field dependencies of photogeneration quantum efficiency holes for the layers of investigated compounds. For all the compounds photogeneration quantum efficiency is strongly field dependent. These dependencies may be approximated by a power law function $\eta \sim E^n$, where factor $n = 3.2$ or 3.1 for **TR1** and **TR2**, and $n = 2.1$ for **TR3**. Such dependence can be explained by Onsager photogeneration mechanisms, and big values of factor n indicate that thermalization distance in photogeneration process is less than the Onsager radius [57]. Compound **TR3** is distinguished with the smallest factor n and the highest values of quantum efficiency, with reaches 0.36 at strong electric field.

Dispersive hole–transport was observed in the layers of **TR1–TR3** coated by solution processing technique (**Fig 8a**). The hole–transit times (t_t) needed for the estimation of hole mobilities were established from the intersection points of two asymptotes of the double–logarithmic plots. The representative electric field dependency of hole–drift mobility for the neat film of **TR2** is shown in **Fig. 8b** and is Poolee–Frenkel type characteristic. Such dependence is commonly observed for organic charge transporting materials in amorphous state due to a disorder. The data of the hole mobility of the neat films of compounds **TR1–TR3** are presented in **Table 5**. The highest hole mobility value is observed for the compound **TR2**. It approached the magnitude of $10^{-2} \text{ cm}^2 \text{ V}^{-1} \text{ s}^{-1}$ at high electric fields.

3.8. Electroluminescent properties

Compounds **TR2** and **TR3** were tested as light emitting materials in the OLED structures based on host–guest system. The blend of poly N-vinyl carbazole (PVK) and 2-(4-tert-butylphenyl)-5-(4-biphenyl)-1,3,4-oxadiazole (PBD) (**Fig. S13**) was used as host, and **TR2** and **TR3** were employed as emitting guest materials. PVK is widely known as hole transporting material. In addition, it possess a large exciton lifetime [58,59]. In order to enable the host system to transport both types of charge carriers i.e. electrons and holes, PBD was mixed with PVK [60,61]. The HOMO and LUMO levels of PVK and PBD are suitable for good energy transfer to the light emitting dopants **TR2** and **TR3** in it (**Fig.9**). UV and PL spectra of the layers of the molecular mixtures PVK:PBD, PVK:PBD:**TR2** and PVK:PBD:**TR3** are given in **Figure S15**. The shape of absorption spectra of the films containing light emitting dopants **TR2** and **TR3** remained similar to those of PVK:PBD film, what means that the **TR2** and **TR3** have no significant influence on the absorbance of active layers. Doping with the guest materials, however, was found to have influence on the PL spectra. The PL maxima of the films of PVK:PBD, PVK:PBD:**TR2** and PVK:PBD:**TR3** were observed at 422nm, 450 nm and 485 nm, respectively.

The electroluminescence (EL) spectra of the fabricated devices I and II are presented in **Figure 10**. The EL intensity maxima of the devices I and II were observed at 463 nm and 515 nm, respectively. Since pure PVK:PBD based devices showed emission maxima at 433 nm [62], and EL emission maxima of the devices I and II were observed at the same wavelengths as PL emission maxima of the films of **TR2** or **TR3**

(Fig. 10), we can conclude that effective excitation energy transfer from the host matrices to the guests takes place in the devices.

Figure 11 shows the current density–voltage characteristics and luminance–voltage characteristics of the devices I and II. The characteristics OLEDs are summarized in the Table 6. The turn–on voltage (V_{on}) of device I was observed at 8 V for electroluminescence of 5.24 cd/m^2 . In the case of device II, the V_{on} was observed at 9.5 V for EL of 1.5 cd/m^2 . The brightness maxima of 1342 and 1221 cd/m^2 were observed at 18 V for devices I and II, respectively, with the maxima of current efficiency in the range of 0.1–0.55 cd/A. CIE chromaticity coordinates of devices I and II were found to be (0.15, 0.13) and (0.21, 0.33), respectively (Fig. S16). The increasing of the bias led to the reduction of the device brightness, followed by the structural degradation. It is known, that V_{on} , brightness and the current efficiency of OLEDs are determined by the thickness of the active layer, injection barriers, balance of charge carriers in the device [63–66]. The thickness of active layer in our OLEDs was 70 nm, which is typical for such kind of devices. OLEDs fabricated in this work do not contain additional hole–transporting or electron transporting layers in addition to PEDOT:PSS. Such additional layers could improve characteristics of the devices and reduce V_{on} . In addition, charge carrier balance in the polymer host–guest matrix devices depends on the amount of light emitting dopant in the matrix blend [67–69]. The optimization of the concentration of TR2 and TR3 in polymer matrix and the application of the additional hole– and/or electron–transporting layers would hopefully provide the possibility of improving the device performance.

4. Conclusions

Star–shaped derivatives of 2,4,6–triphenyl–1,3,5–triazine and carbazole with the different linking topologies of the chromophores were synthesized by a combination of classical and modern synthetic methodologies including Ullmann coupling reaction and Sonogashira cross–coupling reaction. The compounds possess high thermal stability with the temperatures of the onsets of thermal degradation exceeding $460 \text{ }^\circ\text{C}$. They form molecular glasses with glass transition temperatures ranging from 97 to $226 \text{ }^\circ\text{C}$. Solvatochromic behavior of the compounds was investigated studying their solutions in the solvents of different polarity. All the compounds exhibited the positive solvatochromism. Emission color of the solutions could be tuned from deep blue to the yellow with the increase of solvent polarity. The dilute

solutions of the synthesized compounds showed fluorescence quantum yields reaching 0.85 and high Stokes shifts (377-9842 cm^{-1}). All the compounds show linear Stokes shift dependancies on orientation

polarizability, suggesting that they all are strong intramolecular charge transfer fluorophores with highly localized excited state charge separation. The PL decays of the dilute solutions of the compounds were well described by single-exponential fits. Fluorescence quantum yields of the solid films of the compounds were found to range from 0.2 to 0.33. Ionization potentials of the layers of the compounds estimated by photoelectron spectroscopy range 5.49 eV – 5.97 eV. The hole drift mobility of one compound approached the magnitude of $10^{-2} \text{ cm}^2 \text{ V}^{-1} \text{ s}^{-1}$ at high electric fields. The selected compounds were tested as light emitting materials in OLEDs based on host-guest system. The brightness maxima of 1342 and 1221 cd/m^2 were observed at 18 V for devices, with the maxima of current efficiency in the range 0.1 – 0.55 cd/A .

Acknowledgements

This work has been financially supported by the Taiwan-Latvia-Lithuania cooperation project "Synthesis and studies of organic electroactive materials for effective and reliable optoelectronic devices" (grant No TAPLLT1/13). Dr. H.K. Bisoyi is thanked for the valuable advices concerning the synthesis of the compounds. L. Skardziute and S. Jursenas are thanked for the results of the basic photophysical characterization of the compounds. Prof. A. P. Monkman is thanked for providing the conditions for phosphorescence measurements.

- [1] Tang CW, VanSlyke SA. Organic electroluminescent diodes. *Appl Phys Lett* 1987;51:913. doi:10.1063/1.98799.
- [2] Walzer K, Maennig B, Pfeiffer M, Leo K. Highly Efficient Organic Devices Based on Electrically Doped Transport Layers. *Chem Rev* 2007;107:1233–71. doi:10.1021/cr050156n.
- [3] Kanibolotsky AL, Perepichka IF, Skabara PJ. Star-shaped π -conjugated oligomers and their applications in organic electronics and photonics. *Chem Soc Rev* 2010;39:2695. doi:10.1039/b918154g.
- [4] Tang J, Hua J, Wu W, Li J, Jin Z, Long Y, et al. New starburst sensitizer with carbazole antennas for efficient and stable dye-sensitized solar cells. *Energy Environ Sci* 2010;3:1736. doi:10.1039/c0ee00008f.
- [5] Reghu RR, Bisoyi HK, Grazulevicius J V., Anjukandi P, Gaidelis V, Jankauskas V. Air stable electron-transporting and ambipolar bay substituted perylene bisimides. *J Mater Chem* 2011;21:7811. doi:10.1039/c1jm11091h.
- [6] Son KS, Yahiro M, Imai T, Yoshizaki H, Adachi C. Analyzing Bipolar Carrier Transport Characteristics of Diarylamino-Substituted Heterocyclic Compounds in Organic Light-Emitting Diodes by Probing Electroluminescence Spectra. *Chem Mater* 2008;20:4439–46. doi:10.1021/cm8004985.
- [7] Duan L, Qiao J, Sun Y, Qiu Y. Strategies to Design Bipolar Small Molecules for OLEDs: Donor-Acceptor Structure and Non-Donor-Acceptor Structure. *Adv Mater* 2011;23:1137–44. doi:10.1002/adma.201003816.
- [8] Zhu W, Hu M, Yao R, Tian H. A novel family of twisted molecular luminescent materials containing carbazole unit for single-layer organic electroluminescent devices. *J Photochem Photobiol A Chem* 2003;154:169–77. doi:10.1016/S1010-6030(02)00325-8.
- [9] Gong S, Fu Q, Wang Q, Yang C, Zhong C, Qin J, et al. Highly Efficient Deep-Blue Electrophosphorescence Enabled by Solution-Processed Bipolar Tetraarylsilane Host with Both a High Triplet Energy and a High-Lying HOMO Level. *Adv Mater* 2011;23:4956–9. doi:10.1002/adma.201102758.
- [10] Gong S, Sun N, Luo J, Zhong C, Ma D, Qin J, et al. Highly Efficient Simple-Structure Blue and All-Phosphor Warm-White Phosphorescent Organic Light-Emitting Diodes Enabled by Wide-Bandgap Tetraarylsilane-Based Functional Materials. *Adv Funct Mater* 2014;24:5710–8. doi:10.1002/adfm.201400149.
- [11] Moylan CR, Ermer S, Lovejoy SM, McComb I-H, Leung DS, Wortmann R, et al. (Dicyanomethylene)pyran Derivatives with C_{2v} Symmetry: An Unusual Class of Nonlinear Optical

- [12] Sasabe H, Takamatsu J, Motoyama T, Watanabe S, Wagenblast G, Langer N, et al. High-Efficiency Blue and White Organic Light-Emitting Devices Incorporating a Blue Iridium Carbene Complex. *Adv Mater* 2010;22:5003–7. doi:10.1002/adma.201002254.
- [13] Morin J-F, Leclerc M, Adès D, Siove A. Polycarbazoles: 25 Years of Progress. *Macromol Rapid Commun* 2005;26:761–78. doi:10.1002/marc.200500096.
- [14] Michinobu T, Osako H, Shigehara K. Synthesis and Properties of 1,8-Carbazole-Based Conjugated Copolymers. *Polymers (Basel)* 2010;2:159–73. doi:10.3390/polym2030159.
- [15] Blouin N, Leclerc M. Poly(2,7-carbazole)s: Structure–Property Relationships. *Acc Chem Res* 2008;41:1110–9. doi:10.1021/ar800057k.
- [16] Tomkeviciene A, Grazulevicius JV, Kazlauskas K, Gruodis A, Jursenas S, Ke T-H, et al. Impact of Linking Topology on the Properties of Carbazole Trimers and Dimers. *J Phys Chem C* 2011;115:4887–97. doi:10.1021/jp111333v.
- [17] Nenner I. Temporary negative ions and electron affinities of benzene and N-heterocyclic molecules: pyridine, pyridazine, pyrimidine, pyrazine, and s-triazine. *J Chem Phys* 1975;62:1747. doi:10.1063/1.430700.
- [18] Yamamoto T, Watanabe S, Fukumoto H, Sato M, Tanaka T. New Heteroaromatic Polymers Consisting of Alkyl- and Amino-1,3,5-triazine Units. Their Basic Optical Properties and n-Type Time-of-Flight Drift Mobility. *Macromol Rapid Commun* 2006;27:317–21. doi:10.1002/marc.200500773.
- [19] Fink R, Frenz C, Thelakkat M, Schmidt H-W. Aromatic polyethers with 1,3,5-triazine units as hole blocking/electron transport materials in leds. *Macromol Symp* 1998;125:151–5. doi:10.1002/masy.19981250113.
- [20] Zhong H, Xu E, Zeng D, Du J, Sun J, Ren S, et al. New Optoelectronic Materials Based on Bitriazines: Synthesis and Properties. *Org Lett* 2008;10:709–12. doi:10.1021/ol702698r.
- [21] Kulkarni AP, Tonzola CJ, Babel A, Jenekhe SA. Electron Transport Materials for Organic Light-Emitting Diodes. *Chem Mater* 2004;16:4556–73. doi:10.1021/cm049473l.
- [22] Chang C-H, Kuo M-C, Lin W-C, Chen Y-T, Wong K-T, Chou S-H, et al. A dicarbazole–triazine hybrid bipolar host material for highly efficient green phosphorescent OLEDs. *J Mater Chem* 2012;22:3832. doi:10.1039/c2jm14686j.
- [23] Huang W, Tang F, Li B, Su J, Tian H. Large cyano- and triazine-substituted D– π –A– π –D structures as efficient AIEE solid emitters with large two-photon absorption cross sections. *J Mater Chem C* 2014;2:1141. doi:10.1039/c3tc31913j.

- [24] Harwood LM, Moody CJ. *Experimental organic chemistry: principles and practice*. Oxford: Blackwell scientific; 1990. ACCEPTED MANUSCRIPT
- [25] de Mello JC, Wittmann HF, Friend RH. An improved experimental determination of external photoluminescence quantum efficiency. *Adv Mater* 1997;9:230–2. doi:10.1002/adma.19970090308.
- [26] Malinauskas T, Daskeviciene M, Kazlauskas K, Su H-C, Grazulevicius JV, Jursenas S, et al. Multifunctional red phosphorescent bis-cyclometallated iridium complexes based on 2-phenyl-1,2,3-benzotriazole ligand and carbazolyl moieties. *Tetrahedron* 2011;67:1852–61. doi:10.1016/j.tet.2011.01.026.
- [27] Miyamoto E, Yamaguchi Y, Yokoyama M. Ionization potential of organic pigment film by atmospheric photoelectron emission analysis. *Electrography* 1989;28:364–70. doi:http://doi.org/10.11370/isjepj.28.364.
- [28] Montrimas E, Gaidelis V, Pazera A. The discharge kinetics of negatively charged Se electrophotographic layers. *Lith J Phys* 1966;6:569–76.
- [29] Vaezi-Nejad SM. Xerographic time of flight experiment for the determination of drift mobility in high resistivity semiconductors. *Int J Electron* 1987;62:361–84. doi:10.1080/00207218708920988.
- [30] Reghu RR, Grazulevicius J V., Simokaitiene J, Miasojedovas A, Kazlauskas K, Jursenas S, et al. Glass-Forming Carbazolyl and Phenothiazinyl Tetra Substituted Pyrene Derivatives: Photophysical, Electrochemical, and Photoelectrical Properties. *J Phys Chem C* 2012;116:15878–87. doi:10.1021/jp3019952.
- [31] Frisch MJ, Trucks GW, Schlegel, H. B.; Scuseria, G. E.; Robb, M. A.; Cheeseman, J. R.; Scalmani, G.; Barone, V.; Mennucci, B.; Petersson, G. A.; Nakatsuji, H.; Caricato, M.; Li, X.; Hratchian, H. P.; Izmaylov, A. F.; Bloino, J.; Zheng, G.; Sonnenberg, J. L.; Hada, M.; Ehara, M DJ. Gaussian 09, Revision A.02. Gaussian 09, Revis A02 2009.
- [32] Hayami S, Inoue K. Structure and Magnetic Property of the Organic Triradical with Triazine Skeleton; 2,4,6-Tris{p-(N-oxy-N-tert-butylamino)phenyl}triazine. *Chem Lett* 1999;28:545–6. doi:10.1246/cl.1999.545.
- [33] Neugebauer FA, Fischer H. tert.-Butyl-substituierte Carbazole. *Chem Ber* 1972;105:2686–93. doi:10.1002/cber.19721050829.
- [34] Tucker SH. LXXIV.-Iodination in the carbazole series. *J Chem Soc* 1926;129:546. doi:10.1039/jr9262900546.
- [35] Beginn C, Gražulevičius J V., Strohmriegl P, Simmerer J, Haarer D. Synthesis of poly(9-hexyl-3,6-carbazolyleneethynylene) and its model compounds. *Macromol Chem Phys* 1994;195:2353–70. doi:10.1002/macp.1994.021950706.
- [36] Weingarten H. Ullmann Condensation. *J Org Chem* 1964;29:977–8. doi:10.1021/jo01027a529.

- [37] Thorand S, Krause N. Improved Procedures for the Palladium-Catalyzed Coupling of Terminal Alkynes with Aryl Bromides (Sonogashira Coupling) †. *J Org Chem* 1998;63:8551–3. doi:10.1021/jo9808021.
- [38] Zhong H, Lai H, Fang Q. New Conjugated Triazine Based Molecular Materials for Application in Optoelectronic Devices: Design, Synthesis, and Properties. *J Phys Chem C* 2011;115:2423–7. doi:10.1021/jp109806m.
- [39] Tao Y-M, Li H-Y, Xu Q-L, Zhu Y-C, Kang L-C, Zheng Y-X, et al. Synthesis and characterization of efficient luminescent materials based on 2,1,3-benzothiadiazole with carbazole moieties. *Synth Met* 2011;161:718–23. doi:10.1016/j.synthmet.2011.01.020.
- [40] Reichardt C. *Solvents and Solvent Effects in Organic Chemistry*. Weinheim, FRG: Wiley-VCH Verlag GmbH & Co. KGaA; 2002. doi:10.1002/3527601791.
- [41] Reichardt C. Solvatochromic Dyes as Solvent Polarity Indicators. *Chem Rev* 1994;94:2319–58. doi:10.1021/cr00032a005.
- [42] Valeur B. *Molecular Fluorescence*. Weinheim, FRG: Wiley-VCH Verlag GmbH; 2001. doi:10.1002/3527600248.
- [43] Lippert E. Dipolmoment und Elektronenstruktur von angeregten Molekülen. *Zeitschrift Für Naturforsch A* 1955;10:541–5. doi:10.1515/zna-1955-0707.
- [44] Mataga N, Kaifu Y, Koizumi M. Solvent Effects upon Fluorescence Spectra and the Dipolemoments of Excited Molecules. *Bull Chem Soc Jpn* 1956;29:465–70. doi:10.1246/bcsj.29.465.
- [45] Kukhta NA, Simokaitiene J, Volyniuk D, Ostrauskaite J, Grazulevicius JV., Juska G, et al. Effect of linking topology on the properties of star-shaped derivatives of triazine and fluorene. *Synth Met* 2014;195:266–75. doi:10.1016/j.synthmet.2014.06.019.
- [46] Huang B, Yin Z, Ban X, Jiang W, Dai Y, Zhang J, et al. Thermally activated delayed fluorescence of N-phenylcarbazole and triphenylamine functionalised tris(aryl)triazines. *Dye Pigment* 2015;117:141–8. doi:10.1016/j.dyepig.2015.02.014.
- [47] Wang Q, Wallace JU, Lee TY-H, Ou JJ, Tsai Y-T, Huang Y-H, et al. Evaluation of propylene-, meta-, and para-linked triazine and tert-butyltriphenylamine as bipolar hosts for phosphorescent organic light-emitting diodes. *J Mater Chem C* 2013;1:2224. doi:10.1039/c3tc00588g.
- [48] Braslavsky SE. Glossary of terms used in photochemistry, 3rd edition (IUPAC Recommendations 2006). *Pure Appl Chem* 2007;79:293–465. doi:10.1351/pac200779030293.
- [49] Lakowicz JR. *Principles of Fluorescence Spectroscopy*. Boston, MA: Springer US; 2006. doi:10.1007/978-0-387-46312-4.

- [50] Ambrose JF, Nelson RF. Anodic Oxidation Pathways of Carbazoles. *J Electrochem Soc* 1968;115:1159. doi:10.1149/1.2410929.
- [51] Chiu S-K, Chung Y-C, Liou G-S, Su YO. Electrochemical and Spectral Characterizations of 9-Phenylcarbazoles. *J Chinese Chem Soc* 2012;59:331–7. doi:10.1002/jccs.201100601.
- [52] Reghu RR, Grazulevicius JV., Simokaitiene J, Matulaitis T, Miasojedovas A, Kazlauskas K, et al. Glass forming donor-substituted s-triazines: Photophysical and electrochemical properties. *Dye Pigment* 2013;97:412–22. doi:10.1016/j.dyepig.2013.01.017.
- [53] Data P, Pander P, Lapkowski M, Swist A, Soloduch J, Reghu RR, et al. Unusual properties of electropolymerized 2,7- and 3,6- carbazole derivatives. *Electrochim Acta* 2014;128:430–8. doi:10.1016/j.electacta.2013.12.108.
- [54] Lukeš V, Rapta P, Idzik KR, Beckert R, Dunsch L. Charged States of 1,3,5-Triazine Molecules as Models for Star-shaped Molecular Architecture: A DFT and Spectroelectrochemical Study. *J Phys Chem B* 2011;115:3344–53. doi:10.1021/jp111297y.
- [55] Calais J-L. Density-functional theory of atoms and molecules. R.G. Parr and W. Yang, Oxford University Press, New York, Oxford, 1999. *Int J Quantum Chem* 1993;47:101–101. doi:10.1002/qua.560470107.
- [56] Stratmann RE, Scuseria GE, Frisch MJ. An efficient implementation of time-dependent density-functional theory for the calculation of excitation energies of large molecules. *J Chem Phys* 1998;109:8218. doi:10.1063/1.477483.
- [57] Borsenberger PM, Weiss D. *Organic Photoreceptors for Imaging Systems*. New York: CRC Press; 1993.
- [58] Bolink HJ, Santamaria SG, Sudhakar S, Zhen C, Sellinger A. Solution processable phosphorescent dendrimers based on cyclic phosphazenes for use in organic light emitting diodes (OLEDs). *Chem Commun* 2008:618–20. doi:10.1039/B715239F.
- [59] Yap CC, Yahaya M, Salleh MM. Influence of tetrabutylammonium hexafluorophosphate (TBAPF₆) doping level on the performance of organic light emitting diodes based on PVK:PBD blend films. *Curr Appl Phys* 2009;9:722–6. doi:10.1016/j.cap.2008.06.013.
- [60] Huang J, Hou W-J, Li J-H, Li G, Yang Y. Improving the power efficiency of white light-emitting diode by doping electron transport material. *Appl Phys Lett* 2006;89:133509. doi:10.1063/1.2357938.
- [61] Céspedes-Guirao FJ, García-Santamaría S, Fernández-Lázaro F, Sastre-Santos A, Bolink HJ. Efficient electroluminescence from a perylenediimide fluorophore obtained from a simple solution processed OLED. *J Phys D Appl Phys* 2009;42:105106. doi:10.1088/0022-3727/42/10/105106.

- [62] Luszczyńska B, Dobruchowska E, Glowacki I, Ulanski J, Jaiser F, Yang X, et al. Poly(N-vinylcarbazole) doped with a pyrazoloquinoline dye: A deep blue light-emitting composite for light-emitting diode applications. *J Appl Phys* 2006;99:024505. doi:10.1063/1.2162268.
- [63] Cherpak V, Stakhira P, Minaev B, Baryshnikov G, Stromylo E, Helzhynskyy I, et al. Mixing of Phosphorescent and Exciplex Emission in Efficient Organic Electroluminescent Devices. *ACS Appl Mater Interfaces* 2015;7:1219–25. doi:10.1021/am507050g.
- [64] Sun JW, Lee J-H, Moon C-K, Kim K-H, Shin H, Kim J-J. A Fluorescent Organic Light-Emitting Diode with 30% External Quantum Efficiency. *Adv Mater* 2014;26:5684–8. doi:10.1002/adma.201401407.
- [65] Stakhira P, Khomyak S, Cherpak V, Volyniuk D, Simokaitiene J, Tomkeviciene A, et al. Blue organic light-emitting diodes based on pyrazoline phenyl derivative. *Synth Met* 2012;162:352–5. doi:10.1016/j.synthmet.2011.12.017.
- [66] Seo JH, Kim HM, Choi EY, Choi DH, Park JH, Yoo HS, et al. Phosphorescent Organic Light-Emitting Diodes with Simplified Device Architecture. *Jpn J Appl Phys* 2010;49:08JG04. doi:10.1143/JJAP.49.08JG04.
- [67] Lee I-H, Gong M-S. New Fluorescent Blue OLED Host and Dopant Materials Based on the Spirobenzofluorene. *Bull Korean Chem Soc* 2011;32:1475–82. doi:10.5012/bkcs.2011.32.5.1475.
- [68] Zeng L, Lee TY-H, Merkel PB, Chen SH. A new class of non-conjugated bipolar hybrid hosts for phosphorescent organic light-emitting diodes. *J Mater Chem* 2009;19:8772. doi:10.1039/b909787b.
- [69] Zhou X, Qin DS, Pfeiffer M, Blochwitz-Nimoth J, Werner A, Drechsel J, et al. High-efficiency electrophosphorescent organic light-emitting diodes with double light-emitting layers. *Appl Phys Lett* 2002;81:4070. doi:10.1063/1.1522495.

Table 1. Thermal characteristics of compounds **TR1-TR3**.

Table 2. Optical and photophysical properties of the dilute hexane solutions and neat films of compounds **TR1-TR3**.

Table 3. Photophysical characteristics of the dilute solutions of compound **TR1** in the solvents of different polarity.

Table 4. Electrochemical and photoelectrical characteristics of compounds **TR1-TR3**.

Table 5. Hole mobility data of the layers of compounds **TR1-TR3**.

Table 6. EL performances of multi-layered devices with the synthesized emitters. Device: ITO/PEDOT:PSS/PVK:PBD (40 wt %):**guest**(3 wt %)/LiF/Al.

Table 1. Thermal characteristics of compounds **TR1–TR3**.

| Compound | $T_g^{(a)}$, °C | $T_m^{(a)}$, °C | $T_d^{(b)}$, °C |
|-----------------|------------------|------------------|------------------|
| TR1 | 190 | 344 | 528 |
| TR2 | 226 | 448 | 514 |
| TR3 | 97 | – | 467 |

(a) glass transitions (T_g), melting points (T_m) and crystallization temperatures (T_{cr}) were measured by DSC (heating rate of 10 °C/min under nitrogen atmosphere); (b) thermal decomposition temperatures (5 % weight loss temperatures) were measured by TGA (heating rate of 20 °C /min under nitrogen atmosphere)

Table 2. Optical and photophysical properties of the dilute hexane solutions and neat films of compounds **TR1–TR3**.

| Compound | Dilute solution in hexane | | | | | | Solid film | | | | | | E_T , eV ^(g) |
|------------|---------------------------------------|---------------------------------------|--|------------------------------|-------------------------------|------------------------------|---------------------------------------|---------------------------------------|--|------------------------------|-------------------------------|------------------------------|------------------------------|
| | λ_{UV} , nm ^(a) | λ_{PL} , nm ^(a) | $\Delta\tilde{\nu}$, cm ^{-1(b)} | η , % ^(c) | τ , ns ^(d) | CIE (x, y) ^(e) | λ_{UV} , nm ^(a) | λ_{PL} , nm ^(a) | $\Delta\tilde{\nu}$, cm ^{-1(b)} | η , % ^(c) | τ , ns ^(f) | CIE (x, y) ^(e) | |
| TR1 | 389 | 398 | 578 | 83±5 | 2.88 | (0.16, 0.03) | 390 | 462 | 3993 | 33±3 | 1.05 4.70 | (0.16, 0.18) | 2.68 |
| TR2 | 397 | 407 | 616 | 74±5 | 2.82 | (0.16, 0.03) | 400 | 466 | 3538 | 29±3 | 1.29 5.27 | (0.18, 0.22) | 2.65 |
| TR3 | 394 | 400 | 377 | 82±5 | 1.02 | (0.16, 0.06) | 406 | 514 | 5172 | 20±3 | 1.38 4.85 | (0.23, 0.54) | 2.38 |

(a) Peak wavelengths of absorption and emission bands; (b) Stokes' shift; (c) Quantum yields measured using integrating sphere; (d) Fluorescence lifetime estimated for 10^{-5} M hexane solutions ($\lambda_{ex} = 350$ nm) (e) CIE color coordinates; (f) Fluorescence lifetimes estimated for neat films ($\lambda_{ex} = 350$ nm); (g) Values of triplet energies were estimated from the blue-edge maxima of phosphorescence spectra.

Table 3. Photophysical characteristics of the dilute solutions of compound **TR1** in the solvents of different polarity.

| <i>Solvent</i> | $\Delta f^{(a)}$ | $\lambda_{UV},$ nm ^(b) | $\lambda_{PL},$ nm ^(b) | $\Delta\tilde{\nu},$ cm⁻¹ ^(c) | $\eta,$ % ^(d) | $\tau,$ ns ^(e) | χ^2 | $\Gamma,$ ns⁻¹ ^(f) | $k_{NR},$ ns⁻¹ ^(f) |
|------------------------|------------------|---|---|---|------------------------------------|-------------------------------------|----------|--|--|
| Hexane | -0.001 | 389 | 398 | 577.94 | 83±5 | 2.88 | 1.01 | 0.29 | 0.06 |
| Toluene | 0.013 | 385 | 434 | 2929.45 | 76±5 | 3.94 | 1.00 | 0.19 | 0.06 |
| Chloroform | 0.150 | 379 | 480 | 5549.09 | 62±3 | 6.55 | 1.00 | 0.09 | 0.06 |
| Tetrahydrofuran | 0.210 | 378 | 487 | 5918.39 | 53±5 | 7.55 | 1.00 | 0.07 | 0.06 |
| Dichloromethane | 0.217 | 376 | 499 | 6552.97 | 50±5 | 7.59 | 1.00 | 0.07 | 0.07 |
| Acetone | 0.284 | 372 | 520 | 7648.37 | 29±3 | 6.32 | 1.01 | 0.05 | 0.11 |
| Acetonitrile | 0.305 | 370 | 548 | 8776.40 | 23±3 | 4.58 | 1.05 | 0.05 | 0.17 |

(a) Solvent orientation polarizability; (b) Peak wavelengths of absorption and emission bands; (c) Stokes shift; (d)

PL quantum yields measured using integrating sphere; (e) Fluorescence lifetimes estimated in 10^{-5} M solutions (λ_{ex}

= 350 nm); (f) radiative and nonradiative decay rate constants were calculated by the equations $\Gamma = \frac{\Phi}{\tau}$ and

$$k_{NR} = \frac{1}{\tau} - \Gamma.$$

Table 4. Electrochemical and photoelectrical characteristics of compounds **TR1–TR3**.

| <i>Compound</i> | E_{ox} , V ^(a) | E_{red} , V ^(a) | $E_g^{CV(b)}$, eV | IP^{SS} , eV ^(c) | EA^{SS} , eV ^(d) | $E_g^{opt(e)}$, eV | IP^{EP} , eV ^(f) | E_{HOMO} , eV ^(g) | E_{LUMO} , eV ^(g) |
|-----------------|--------------------------------|---------------------------------|-----------------------|----------------------------------|----------------------------------|------------------------|----------------------------------|-----------------------------------|-----------------------------------|
| TR1 | 0.89 | -1.74 | 2.63 | 5.49 | 2.86 | 2.96 | 5.95 | -5.71 | -2.39 |
| TR2 | 1.10 | -1.77 | 2.87 | 5.70 | 2.83 | 2.90 | 5.97 | -5.63 | -2.37 |
| TR3 | 0.77 | – | – | 5.37 | – | 2.85 | 5.49 | -5.67 | -2.51 |

(a) for the **TR1** and **TR3** onset of the first oxidation potential, for **TR2** halfwave oxidation

potential; E_{red} is halfwave reduction potential; (b) calculated using equation $E_g^{CV} = E_{ox} - E_{red}$;

(c) calculated using equation $IP^{CV} = 4.8 + E_{ox\ vs\ FC}$; (d) calculated using equation $EA^{CV} = 4.8 +$

$E_{red\ vs\ FC}$; (e) E_g^{opt} was calculated using equation $E_g^{opt} = 1239.75/\lambda$ ($\lambda_{TR1} = 418\ nm$, $\lambda_{TR2} = 427$

nm , $\lambda_{TR3} = 435\ nm$ (from UV spectra)); (f) ionization potentials measured by electron

photoemission spectrometry (g) HOMO and LUMO energies were calculated using rB3LYP/6-

311g (d,p) method.

Table 5. Hole mobility data of the layers of compounds **TR1–TR3**.

| <i>Compound</i> | <i>d</i> , $\mu\text{m}^{(a)}$ | μ_0 , $\text{cm}^2 \text{V}^{-1}\text{s}^{-1(b)}$ | μ , $\text{cm}^2 \text{V}^{-1}\text{s}^{-1(c)}$ | α , $\text{cm}^{1/2} \text{V}^{-1/2(d)}$ |
|-----------------|--------------------------------|--|--|--|
| TR1 | 1.5 | | $2 \cdot 10^{-3}$ | |
| TR2 | 2.1 | $1.4 \cdot 10^{-4}$ | $7.5 \cdot 10^{-3}$ | 0.004 |
| TR3 | 2.0 | | $3 \cdot 10^{-3}$ | |

(a) Layer thickness; (b) mobility value at zero field strength; (c) mobility value at $6.4 \cdot 10^5$ V/cm field strength; (d) the Poolee–Frenkel parameter.

Table 6. EL performances of multi-layered devices with the synthesized emitters. Device: ITO/PEDOT:PSS/PVK:PBD (40 wt %):**guest**(3 wt %)/LiF/Al.

| <i>Device</i> | V_{on} , V ^(a) | EL_{max} , nm ^(b) | <i>Brightness</i> , cd/m ^{2(c)} | <i>C.E.</i> , cd/A ^(d) | <i>CIE</i> , (x,y) ^(e) |
|-----------------------|-----------------------------|--------------------------------|---|--------------------------------------|--------------------------------------|
| <i>I (guest TR2)</i> | 8 | 463 | 1342 | 0.51 | (0.15, 0.13) |
| <i>II (guest TR3)</i> | 9.5 | 515 | 1221 | 0.46 | (0.21, 0.33) |

(a) Turn on voltage; (b) Electroluminescence maxima; (c) Brightness maxima at 18 V; (d) Current efficiency; (e)

CIE color coordinates.

Scheme 1. Synthetic routes to **TR1** – **TR3**.

Figure 1. UV absorption and photoluminescence spectra of 10^{-5} M hexane solutions (solid lines), thin films (dashed lines) and phosphorescence spectra (short dashed lines) of compounds **TR1-TR3**.

Figure 2. Photoluminescence spectra of 10^{-5} M solutions of compound **TR1** in hexane, toluene, chloroform, tetrahydrofuran, dichloromethane, acetone and acetonitrile solutions ($\lambda_{\text{ex}} = 350$ nm).

Figure 3. a) Dependencies of radiative (circles) and nonradiative (rhombus) decay rate (a), of PL quantum yield (squares) and of Stokes shift (triangles) (b) on orientation polarizability (Δf) of **TR1**. Dashed lines stand for the linear fit.

Figure 4. PL decays of neat films of compounds **TR1-TR3**.

Figure 5. Cyclic voltammetry scans of dilute $1 \mu\text{g/ml}$ solutions of compounds **TR1-TR3**.

Measurement conditions: $0.1 \text{ M Bu}_4\text{NBF}_6/\text{dichloromethane}$ electrolyte, scan rate 100 mV/s .

Figure 6. The frontier orbitals of compounds **TR1-TR3**.

Figure 7. Field dependencies of the holes photogeneration quantum efficiency in the layers of **TR1-TR3**.

Figure 8. (a) XTOF transients for the neat film of **TR2**. Arrow mark indicate transit time of holes at the respective surface voltage; (b) Electric field dependencies of hole–drift mobilities of the amorphous layer of **TR2**.

Figure 9. Energy diagrams of the devices I (a) and II (b).

Figure 10. Normalized electroluminescence spectra (solid lines) of devices I and II and PL spectra of neat films (dashed lines) of **TR2** and **TR3**.

Figure 11. Current density-voltage and luminance-voltage characteristics (a), current efficiency – current density characteristic (b) of the devices I and II.

